Bull. Disas. Prev. Res. Inst., Kyoto Univ., Vol. 43, Part 1, No. 372, March, 1993

Mechanism of Landslides Triggered by the 1990 Iran Earthquake

By Zieaoddin SHOAEI and Kyoji SASSA

(Manuscript received on October 6, 1992, revised on January 12, 1993)

Abstract

The June 1990 Manjil earthquake that shocked Gilan and Zanjan provinces of Iran (in north and northwestern Iran) provoked several landslides in the region over the south part of Alborz mountains. Two of these landslides (the Galdian and the Fatalak landslides) were selected to be discussed in this paper.

Samples were collected from these landslides. Shear tests were carried our using the newly-developed cyclic loading ring shear apparatus. The stress condition in slopes during earthquake was approximately reproduced. The results of the tests were used for interpreting the mechanism of high velocity motion in the Fatalak landslide and in the upper part of Galdian landslide during the main shock, and the intermittent low velocity motion in the lower part of the Galdian landslide during the following two weeks after the main shock.

1. Introduction

At 00 : 30 AM, 20 June 1990 a disastrous earthquake occurred in the north and northwest of Iran in Gilan and Zanjan Provinces. The epicenter of the main shock was located about 200 km northwest of Tehran, near Manjil city. Duration of the main shock was about 15 seconds and was followed by aftershocks during the following two weeks after the main shock. The magnitude of the main shock reported by Niazi and Bozorgnia[1] was mb (body-wave magnitude) 6.4 and Ms (suface-wave magnitude) 7.7. The magnitudes of the aftershocks were about mb 4.1 to 5.8. Locations of the epicenters of the main shock and the aftershocks are indicated in **Fig. 1.** The tremor of the main shock was felt over a wide area covering 600,000 km^2. The earthquake caused extensive damage in the densely-populated area near the epicenter. More than 35,000 inhabitants were killed mostly in Roodbar and its surrounding villages, 110,000 people were injured, and more than 500,000 lost their houses that placed this event as one of the most tragic disasters in recent decades in Iran.

A concomitant type of catastrophic event was landslides. Strong ground motion triggered landslides of various scales in about 140 places around and near the epicenter of the main shock of the earthquake. Locations of some of these landslides are indicated in **Fig. 1.** Fortunately most of them were located in places far from the residential areas, causing damage only to the cultivating roads, farms and so on. However, about 127 inhabitants were killed in the Fatalak landslide. For interpreting the mechanism of fast and slow motion of landslides triggered by the earthquake, two landslides were selected for investigation : the Fatalak land-

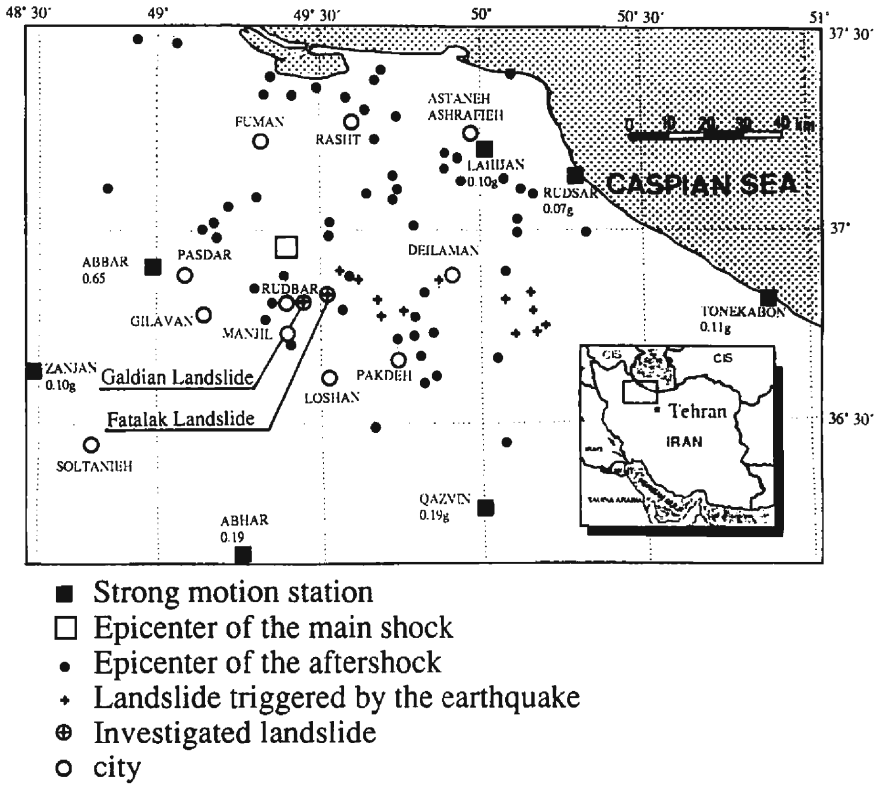

Fig. 1 Location map of the strong-motion stations and epicenters of the main shock and of the aftershocks (after M. Niazi, et al, 1992), triggered landslides during the 1990 Iran earthquake and the investigated landslides.

slide that occurred with high velocity and simultaneously with the main shock and the Galdian landslide in which the failure occurred with high velocity at its upper part during the main shock followed by intermittent slow motion at its lower part during the following two weeks after the main shock. Samples were collected from the bottom part of scarps because they were part of the sliding surface.

2. Landslides Triggered by the Earthquake Chosen for Investigation

2. 1 Galdian Landslide

The biggest landslide in scale at the time of the Manjil earthquake was the Galdian landslide that occurred at the eastern flank of Sefidrood valley and near the city of Roodbar as indicated in **Fig. 2.** This landslide started from the slopes near the Galdian village and its direction extended along the wide U-shaped valley and then veered at the middle part of the sliding area. **Fig. 2** is a contour map of the Galdian landslide. **Photo. 1** is a bird's-eye view of

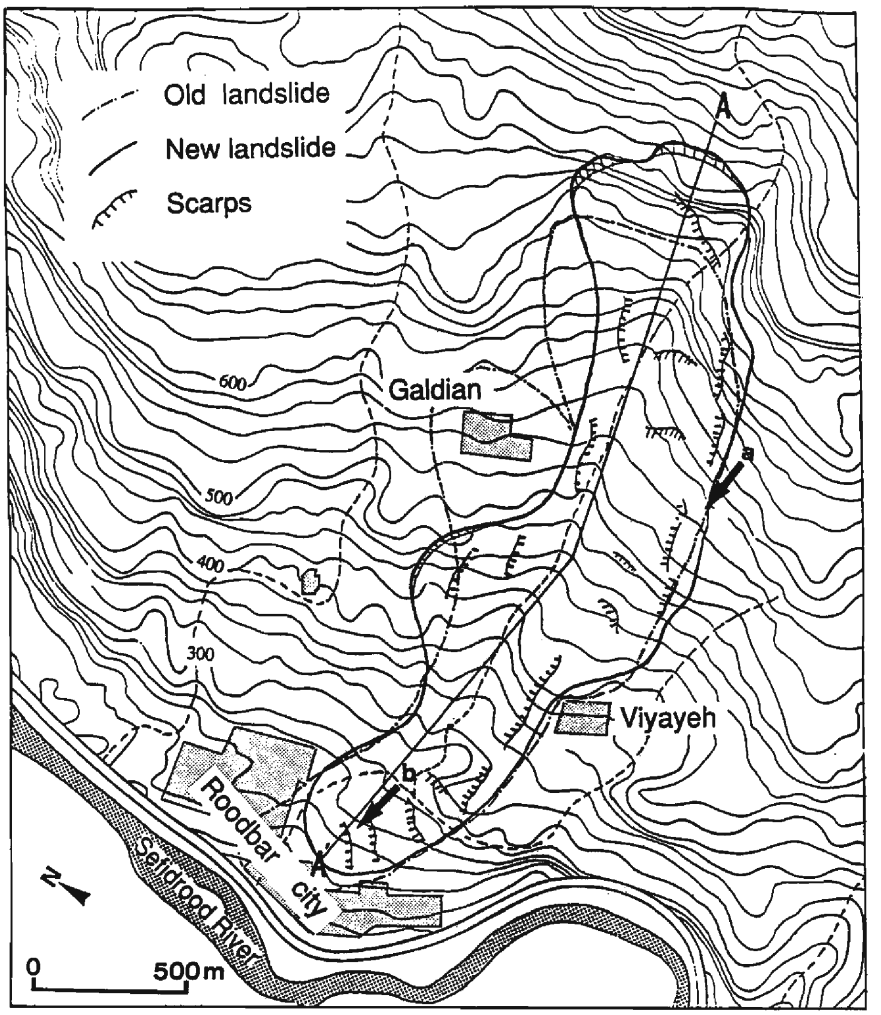

Fig. 2 Contour map of the Galdian landslide, the new sliding area is encircled by solid line and the old landslide is indicated by dotted line, arrow "a" and arrow "b" indicate directions of Photo. 2 and Photo. 3 respectively.

this landslide. The displaced soils encompassed an area 250 to 500m wide and 2800m long. As investigated by M. A. Nogol Sadat[2] the average depth of deposited weathered soils in this area was about 45m, and the sliding surface was formed at about 20–25m depth of the sediments. This estimation was in agreement with the field observation by Z. Shoaei. The volume of the moved mass was about 25 million m^3. A longitudinal cross section (A–A′) of this landslide is shown in **Fig. 3** with the direction of this section indicated in **Fig. 2**.

The initial landslide at the headscarp (approximately shown by mesh in **Fig. 3**) began to move suddenly and simultaneously with the main shock and caused breaking of the pipeline at

Photo. 1 Bird's-eye view of the Galdian landslide (taken on July 1991), dashed line indicates the border of the new landslide.

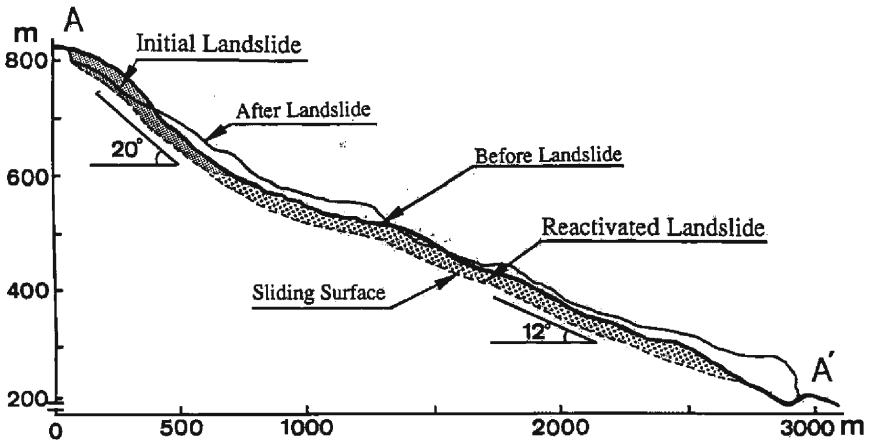

Fig. 3 Longitudinal section of the Galdian landslide (the direction of section is shown in Fig. 2).

the headscarp. According to accounts of witnesses the motion was not visible in the downhill area during the day after the main shock, but by the third day the motion was being felt by surface motion and tilting of trees. The intermittent sliding continued for about two weeks after the main shock. **Photo. 2** is a close up of the stepped tensional feature of the surface of landslide, arrow "a" in **Fig. 2** indicates the direction of photo. The sliding stopped at a location very close to a residential area of Roodbar city where an uplifting had formed (**Photo. 3**), arrow "b" in **Fig. 2** indicates the direction of this photo.

The displaced material was the weathered soil that separated from the geological formation ranging from Triassic to middle Jurassic. This formation is locally referred to as the Shemshak formation, and is composed of siltstone, shale and mudstone with intercalation of coal-bearing thin layers. This formation is very susceptible to weathering, yielding tetritus of fine grained soil and, in some cases, clayey soil with boulders and pebbles. The intercalation of impermeable layers within the prevailing high permeable layers in the Shemshak formation has resulted in outlets of ground water as springs at various elevations of the slopes in this area. Inhabitants had used this spring water as the main source of irrigation of olive tree groves on the hillside, but most of these springs were destroyed during the main shock. These springs affected the hydrological system of the overlaid deposit in the slope. A complicated and little-known hydrological system made it very difficult to know the position of ground water. However, the sliding surface was presumably formed in a saturated or almost saturated zone above one of the impermeable layers.

Variation of weathering susceptibility of the source rocks resulted in different textures of soils in the Galdian landslide area. The weathered silty-sand soil including pebbles and boulders was the most prevailing texture. Samples were collected from the fine grained soil at the bottom of scarps in the top and middle parts of the landslide area.

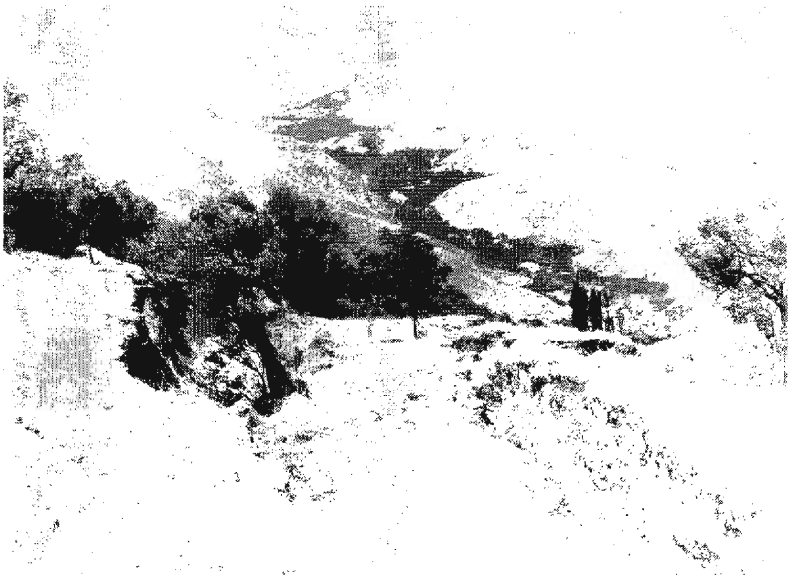

Photo. 2 Stepped-tensional feature of the Galdian landslide (the direction of Photo. is indicated as arrow "a" in Fig. 2).

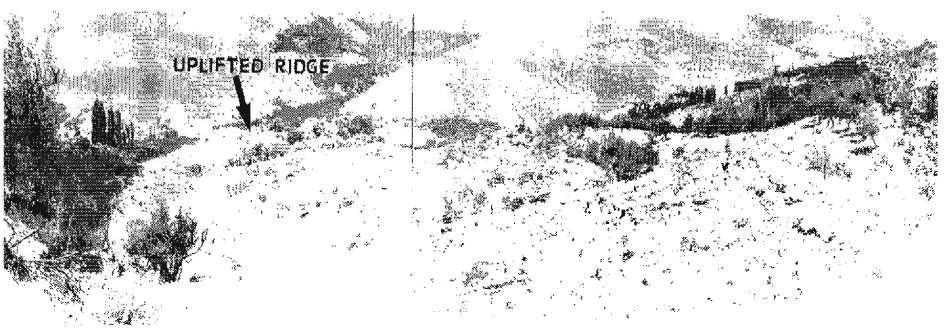

Photo. 3 Uplifted ridge occurred at a point close to Roodbar city (direction of Photo. is indicated as arrow "b" in Fig. 2).

2. 2 Fatalak Landslide

The most catastrophic landslide event during the Manjil earthquake was the Fatalak landslide (east of Roodbar, **Fig. 1**). According to the accounts of witnesses, the landslide moved rapidly and completely buried the Fatalak village.

The landslide encompassed an area 400m long and 300m wide. The depth of sliding surface was about 20m on the average[2]. The volume of moved soil was about 2 million m^3. A frontal view of the Fatalak landslide is shown in **Photo. 4**, and **Photo. 5** is a close-up view of the headscarp. Apparently the Fatalak landslide consisted of two parts : a smaller headscarp (about 20m) with steep slope (**Fig. 4–a**), and a higher headscarp (about 40m) with relatively

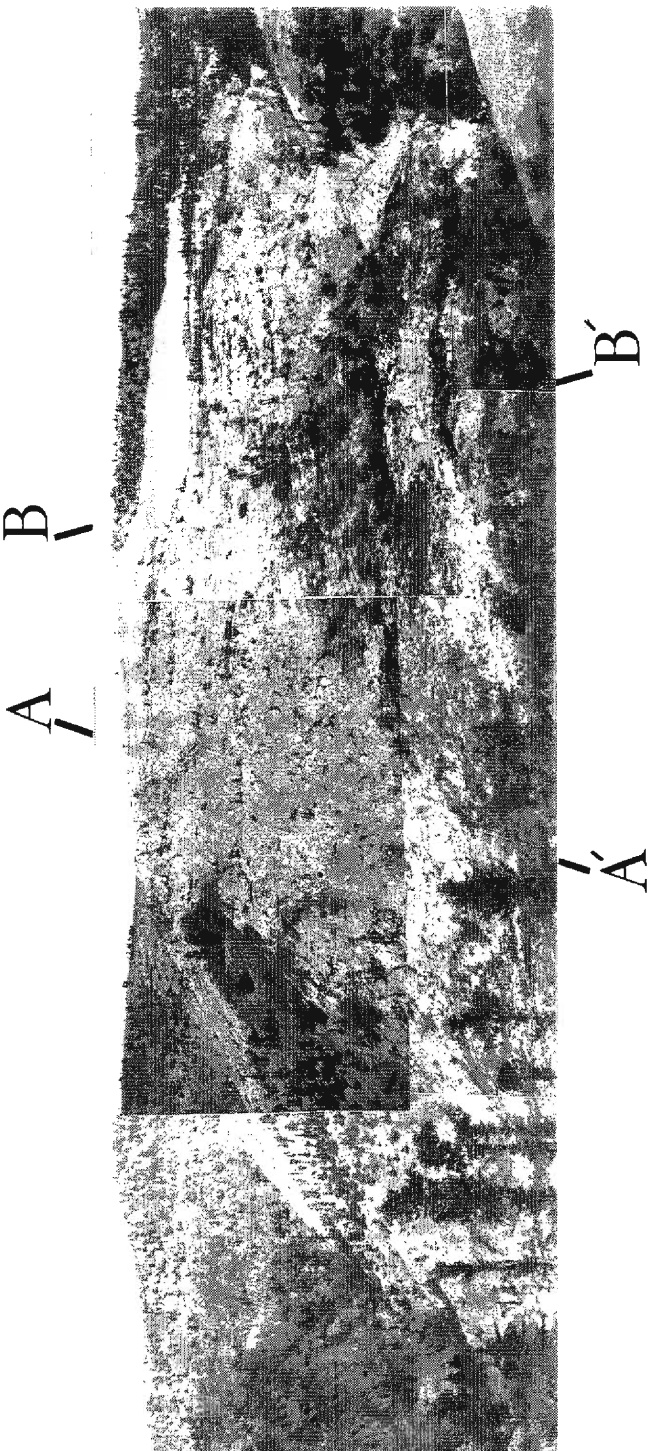

Photo. 4 Front view of the Fatalak landslide, AA′ and BB′ indicate the directions of sections in Fig. 4.

Photo. 5 A close up view of headscarp of the Fatalak landslide (arrow indicates two persons as scale).

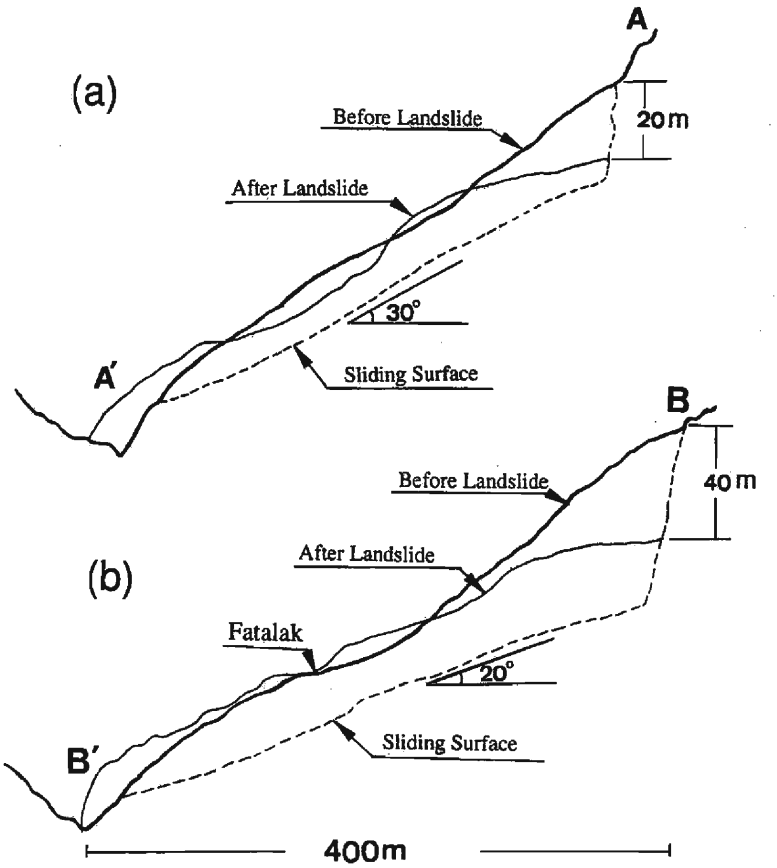

Fig. 4 Approximate longitudinal sections of the two directions of the Fatalak landslide (directions are shown in Photo. 4).

gentle slope (**Fig. 4–b**). The directions of sections are indicated in **Photo. 4.** The headscarp of landslide was composed of hard conglomerate with well–defined deep fractures that could be responsible for its weakness during the failure. The moved material at the middle and lower parts was composed of weathered soils with various sizes of boulders included. The source of the weathered material was limestone, siltstone and shale of the Triassic and Jurassic formations. Samples were collected from the fine grained soil at the bottom of scarps at the top and middle parts of landslide area.

3. Design of a New Cyclic Loading High–Speed Ring Shear Apparatus

At about the same time as the development of a high–velocity ring shear apparatus by Hungr and Morgenstern[3] in 1984, a high–speed ring shear apparatus was developed for debris

flow study by Sassa *et al.*[4] with the maximum normal stress of 0.4 kgf/cm^2, and the maximum shear speed of 90 cm/sec. A high-speed high-stress ring shear apparatus was produced in 1989 by Sassa *et al.*[5] with the maximum normal stress of 3.8 kgf/cm^2 and the maximum shear speed of 100 cm/sec. These series of ring shear apparatus were capable of constant-speed shearing similar to the conventional ring shear apparatus. However, to simulate the behavior of earthquake-induced-landslides, cyclic shear stress loading and cyclic normal stress loading is necessary. In 1992 Sassa[6] developed a cyclic loading high-speed ring shear apparatus. This apparatus was used for this research, and its design is briefly explained below.

3.1 General Design

Fig. 5 is the diagram of the apparatus. Sample (L) is placed in the ring shear box. The outside of the ring shear box is made of transparent acrylic resin, so that the sample is visible during the tests. The lower half rotates by a servo-motor (rotating parts are marked with dots in the figure), while its upper half (slightly moving parts as marked with inclined dash in the figure) is retained to the stable base by a load cell (I) to measure shear resistance.

The front view of the apparatus is presented in **Photo. 6**. The lower half of the shear box and the sample after shearing are shown in **Photo. 7**. The inside diameter of the shear box is 21.0 cm, the outside diameter is 31.0 cm and the shear area is 408.4 cm^2. The depth of the shear box under the shearing plane is 3.8 cm, the height over the shear plane is 6.0 cm and the height of sample above the shear plane depends on the volume change during consolidation. Six porous metal disks (metal filters) are fixed to the base and the loading plate (J), to allow drainage. Needles are fixed to the base and the loading plate in order to prevent the slipping of the two halves of the sample inside the shear box. The rubber edges (M) are affixed to the upper edges of the inner and the outer rings in order to prevent the leakage of sample during the shearing. A transparent water tank (N) surrounds the sample box for the tests of saturated samples.

3.2 Loading System

Static and cyclic normal stress is generated by an air piston (B in **Fig. 5**) controlled by an electric servo-air-valve (electric pneumatic converter and relay booster). An electric control signal is supplied by a personal computer. The electric servo-air-valve gives a certain air pressure corresponding to the control signal. Feedback from the load cell of normal stress is given to the servo-control amplifier. In the cyclic shear loading tests, an input of electric control signal from the computer is given to the servo-motor (V). The motor supplies a certain torque corresponding to the input signal (feedback from the torque meter of the apparatus is not given to the computer). The servo-motor produces constant speed shearing by a control signal during the constant speed test. In the constant volume test, a high precision gap sensor (II) is fixed to detect the difference of distance between the loading plate and the upper lid of the sample box by which a change of 0.002 mm is detected. The feedback of this sensor is given to the normal stress servo-control amplifier. Fixing the position of the loading plate is automatically controlled by increasing or decreasing the air pressure of piston (B) proportional to input feedback signal.

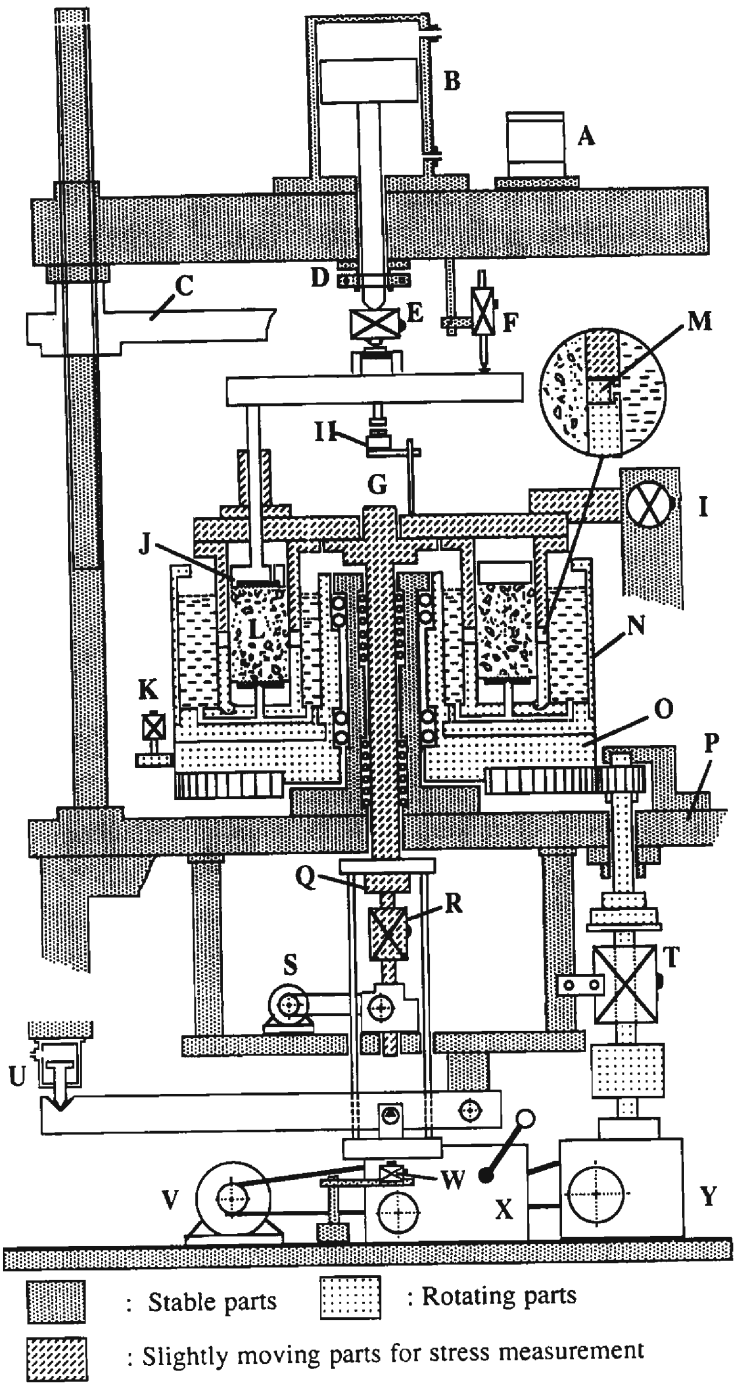

Fig. 5 Section diagram of newly–developed cyclic ring shear apparatus.

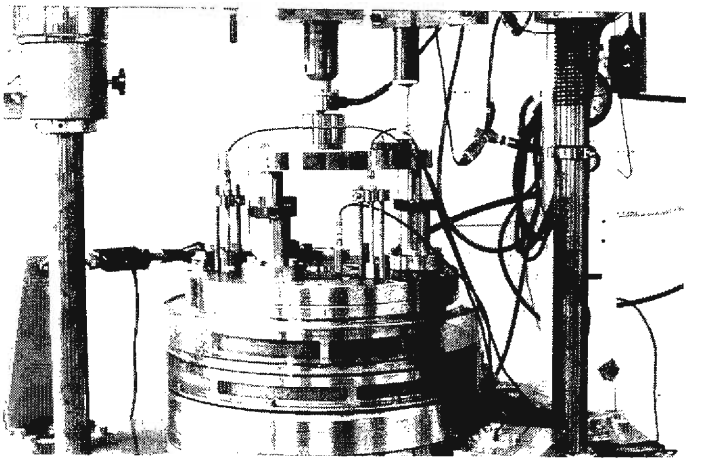

Photo. 6 Frontal view of the cyclic ring shear apparatus.

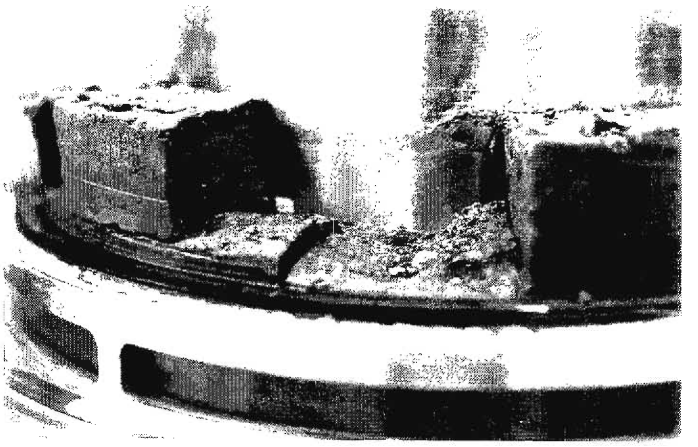

Photo. 7 The lower part of the sample box. The sample is from the Galdian landslide after the tests. The upper part of the sample box and a part of sample were removed to show the shear zone.

3. 3 Monitoring System

Vertical load is measured by load cell (E), and the friction between the sample and the sides of the upper shear box is measured by load cell (R). The difference of the values of load cell (E) and load cell (R) gives the correct vertical load on the shear plane. To keep the gear of the gap control system below the load cell (R) and the rotary joint (Q) in the compression position, a dead weight is applied by an air regulator (U). Shear force is transmitted through the shear plane from the rotating lower half of the shear box and the shear load is measured by the load cell (I). The shear torque given by a servo-motor is monitored by a torque con-

verter (T). The horizontal displacement is monitored by a rotary transducer (K). The variation of sample height is monitored through the loading plate by a linear transducer (F).

3.4 Gap Control

Load cell (R) slightly deforms during cyclic loading in proportion to the change of friction of the sample in the upper half of shear box. The gap of the upper ring and the lower ring is maintained automatically by a servo–motor (S) using the feedback signal from the high precision gap sensor (W) which detects a change of 0.002 mm. A rubber edge (Rubber Hardness Index, 45° JIS K) of 9 mm thickness (M) is affixed to the upper ring. The rubber edge is constantly under about 40 kgf pressure in order to prevent the leakage of sample during cyclic loading and high speed shearing. Te surface of the rubber edge is coated with Teflon in order to decrease the friction between the metal and the rubber edge. Shear friction between the rubber edge of the upper half and the stainless steel edge of the lower half of the sample box during shearing is about 0.04 kgf/cm^2 in terms of shearing stress.

3.5 Shear Speed

Shear speed of this apparatus can be changed from 0.0002 cm/sec to 150 cm/sec using three steps of gears and two sets of pulleys. In the torque control state as well as the speed control state, the maximum shear speed is limited by the capacity of the motor. The maximum shear speed is 150 cm/sec at 1 : 1 pulleys and 37 cm/sec at 1 : 4 pulleys. In this test series, the frequency of 0.1 Hz. of cyclic loading was adopted, which is nearly one order less than that in real earthquakes. Accordingly, a setting of 37 cm/sec for the maximum speed was selected, which is about one order less than the speed of real fast landslides.

4. Tests Conditions and Tests Procedures

4.1 Tests Conditions

Evaluation of true behavior of in–situ soil deposits during an earthquake is very desirable. For an accurate assessment of the effective factors in the occurrence of landslides during earthquakes and prediction of further motion, reproducing stress conditions in the slope during an earthquake is necessary. The directions of seismic stresses in the Galdian landslide and the Fatalak landslide were not known. Therefore, seismic stress parallel to the slope was assumed. This is a simplification, but it has the advantage of being constant during cyclic loading and for series of other tests. The relationship between the stress in the cyclic loading ring shear test and the stress during an earthquake is illustrated in the field stress condition of **Fig. 6–a**) and also in the stress diagram of **Fig. 6–b**). As will be presented in Figs. 11 and 14 later, the normal stress was not completely constant during the test, so a small normal stress increment ($d\sigma_f$) was drawn in **Fig. 6–b**. For simulating a seismic stress, when a stress increment (kw) is applied, so that the stress path may cross the failure envelope and go over it, failure should start at the stress increment of $k_f w$ in which the stress path just reaches the failure envelope. Further stress increment ($kw-k_f w$) is then consumed by acceleration, and the stress on the shear plane remains on the failure envelope. An increment of the shear stress on the shear

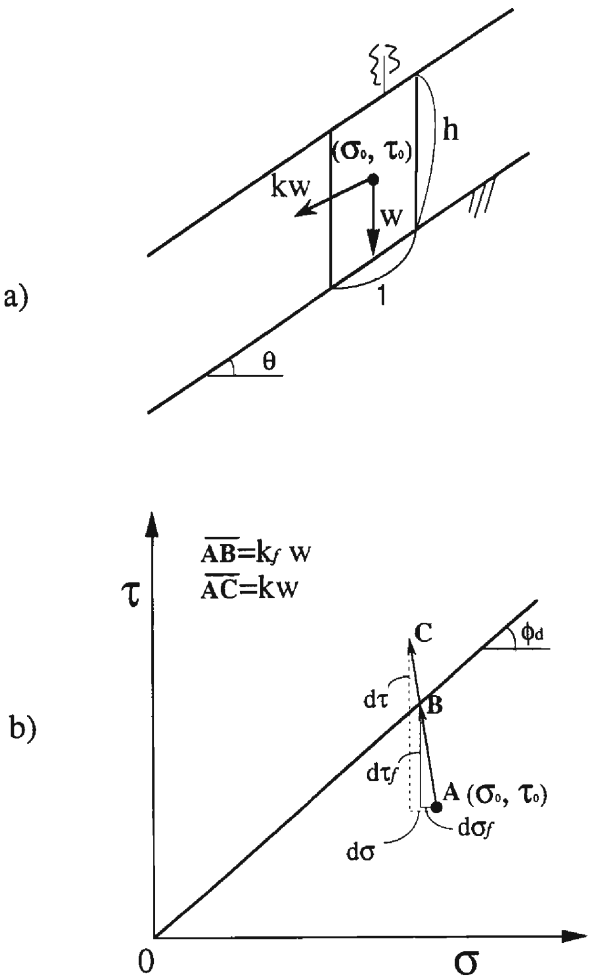

σ_0, τ_0 : Initial stress

W : Self weight of the soil column

h : Depth of the sliding surface

kW : Seismic stress

k_f W : Seismic stress necessary to cause failure

$d\tau_f$: Increment of shear stress on the shear plane (shear resistance) at failure

$d\sigma_f$: Increment of normal stress on the shear plane at failure

ϕ_d : Dynamic friction angle

θ : Slope angle

$d\tau$: Shear stress component of seismic stress (kW)

$d\sigma$: Normal stress component of seismic stress (kW)

Fig. 6 Stress condition during earthquake in the field and stress condition of the cyclic loading ring shear test in the stress diagram.

plane at failure ($d\tau_f$) is the value that is monitored by the load cell (I), and $d\sigma_f$ is the normal stress increment from the initial stress on the shear plane at failure.

4.2 Test Procedures

Some properties of the samples in the field and during the tests are listed in **Table 1**. Grain size distribution curves of the samples used from the Fatalak and the Galdian landslides are shown in **Fig. 7**, and **Fig. 8** is the X-ray diffraction analysis of these samples. The peak intensities of clay minerals (montmorillonite, kaolinite, illite as found at 6–13 degrees) in the sample from the Galdian landslide are higher than that from the Fatalak landslide, which confirmed that the clay minerals in the Galdian sample were more abundant than in the Fatalak sample. For sample preparation, the samples were mixed with water and stirred for a few hours and left for one day for dispersion of soil aggregates, then were stirred again to obtain a slurry sample. The buckets of samples were shaken to release the entrapped air bubbles inside the pores and then the samples were put in the shear box that had been half-filled with water in order to avoid air entrapment. At the first stage of each test, the sample was consolidated under a normal stress corresponding to its initial normal stress in the field. After completion of consolidation, the sample was slowly subjected to shear stress corresponding to its initial shear stress in the field. In the second stage, cyclic shear loading was performed while the total normal stress was kept almost constant by using the servo-amplifier. Twenty cycles of shear loading at a frequency of 0.1 Hz was carried out. A monotonic loading test under constant normal stress and constant shearing speed was also performed to get the residual state of

Table 1 Some physical properties of the sumples in the field and during the tests.

Sample	G_s	γ_t(gf/cm^3) (in the field)	Test stage	γ_d(gf/cm^3) (in the tests)	e
Fatalak Landslide	2.74	1.96	No.(1-2) Consolidation (2.88 kgf/cm^2)	1.69	0.475
			No.(1-3) Cyclic shear test	1.89	0.459
Galdian Landslide	2.73	2.05	No.(2-2) Consolidation (3.07 kgf/cm^2)	1.84	0.479
			No.(2-3) Cyclic shear test	1.87	0.456
			No.(2-4) Constant speed shearing to get the residual strength state	1.88	0.448
			No.(2-5) Cyclic shear test (residual strength state)	1.88	0.448

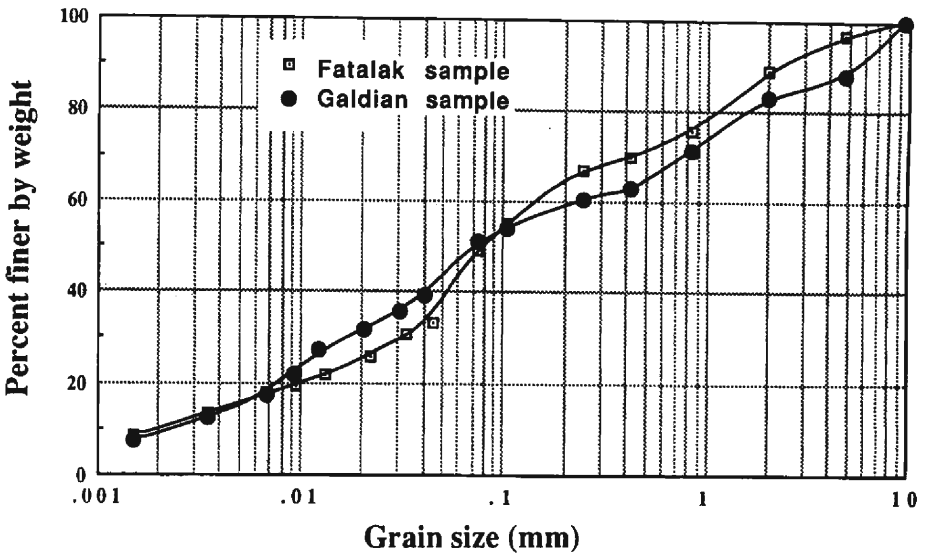

Fig. 7 Grain-size distribution curves of the Fatalak and the Galdian landslides samples.

the sample, then without changing the sample the cyclic shear loading test was repeated.

5. Test Results

5.1 Fatalak Landslide

After consolidation (test No. 1-2) and initial shear stress loading, the cyclic shear test was carried out. The variation of normal stress was kept less than 0.2 kgf/cm^2 during the test. **Fig. 9** (test No. 1-3) shows the stress path of the 1st, 2nd and final (20th) cycles. Failure occurred in the first cycle. The shear displacement after failure was about 30m during the 20 cycles. Logarithm of shear displacement is used in **Fig. 10** (test No. 1-3) to present the variation of sample height, normal stress, shear stress and shear velocity. Time series data of the variation of sample height, normal and shear stresses, shear displacement and shear velocity are presented in **Fig. 11** (test No. 1-3). As mentioned above, failure took place in the first cycle and the shearing velocity changed in the range of 0 to 23 cm/sec in proportion to the value of cyclic loaded shear stress.

5.2 Galdian Landslide

After completion of consolidation (test No. 2-2) and initial shear stress loading, the cyclic shear loading test was performed. Failure took place in the first cycle. The variation of normal stress during cyclic shear loading was kept less than 0.2 kgf/cm^2 during the test. **Fig. 12** (test No. 2-3) shows the stress path of the 1st, 2nd and 20th cycles of this test. Logarithm of shear displacement is used in **Fig. 13** (test No. 2-3) to present the variation of sample

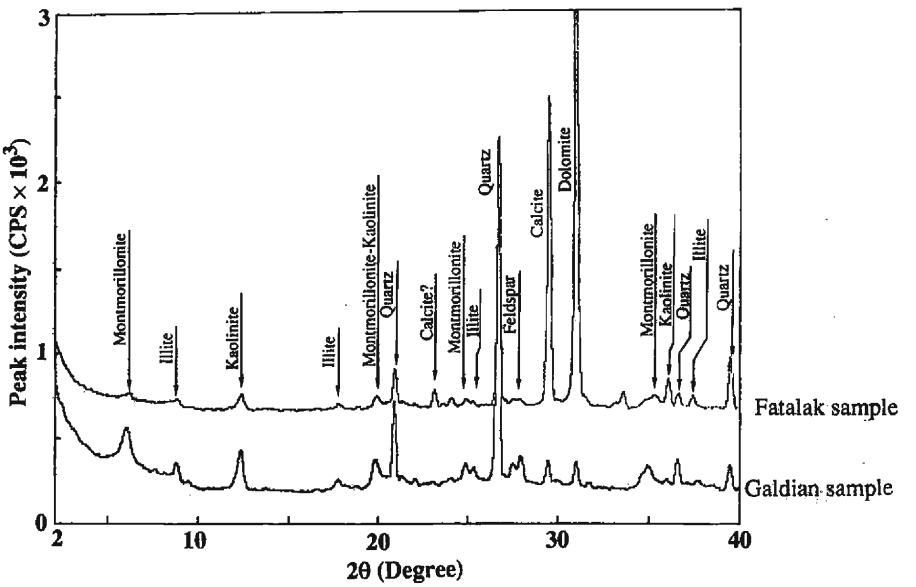

Fig. 8 X-ray diffraction analysis of the Fatalak and the Galdian landslides samples.

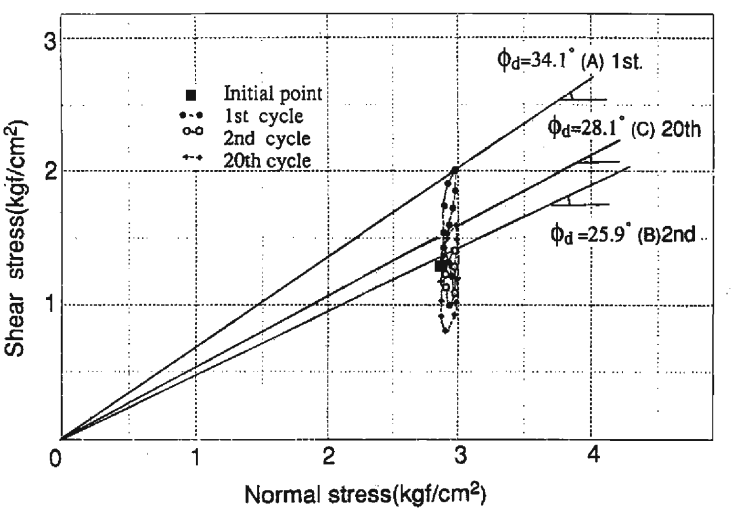

Fig. 9 Stress path of the 1st, 2nd and 20th cycles in the cyclic shear test of the Fatalak sample at the peak strength state (test No. 1-3).

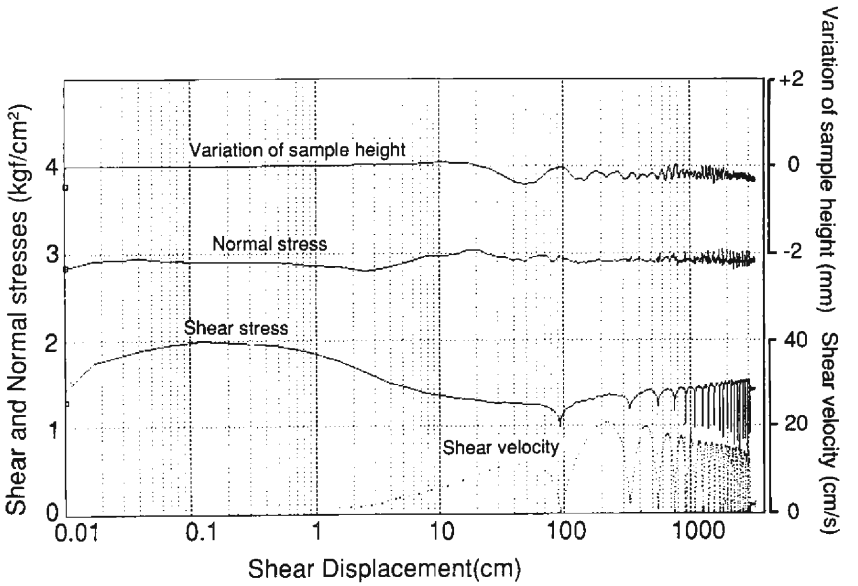

Fig. 10 Shear displacement (Log L) versus variation of sample height, normal stress, shear resistance and shear velocity in the cyclic shear stress loading test of the Fatalak sample at the peak strength state (test No. 1–3).

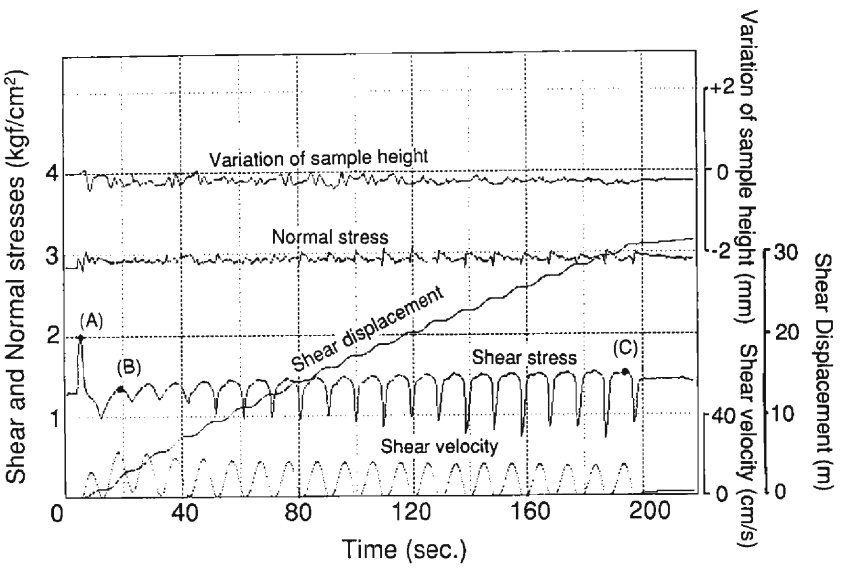

Fig. 11 Time series data of variation of sample height, normal stress, shear displacement, shear velocity in the cyclic shear stress loading test of the Fatalak sample at the peak strength state (test No. 1–3).

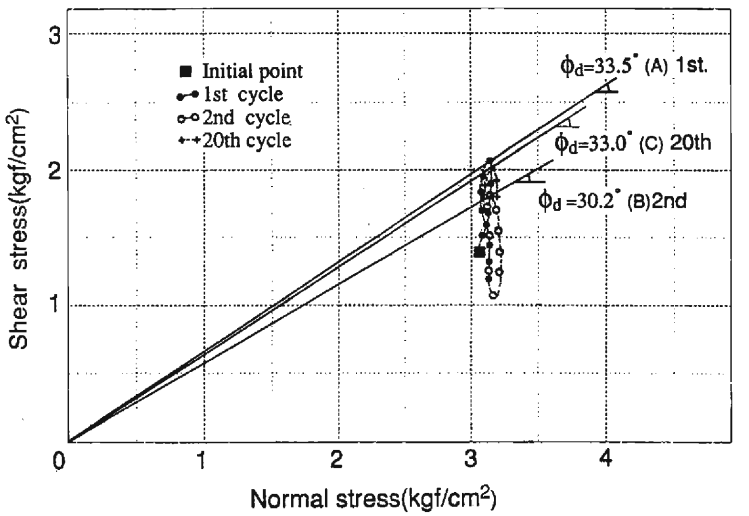

Fig. 12 Stress path of the 1st, 2nd and 20th cycles in the cyclic shear test of the Galdian sample at the peak strength state (test No. 2–3).

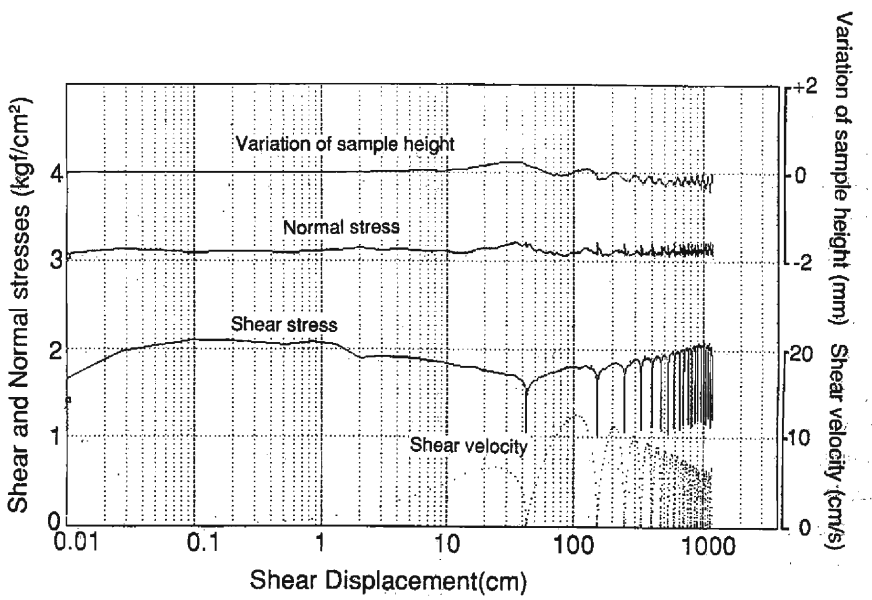

Fig. 13 Shear displacement (Log L) versus variation of sample height, normal stress, shear resistance and shear velocity in the cyclic shear stress loading test of the Galdian sample at the peak strength state (test No. 2–3).

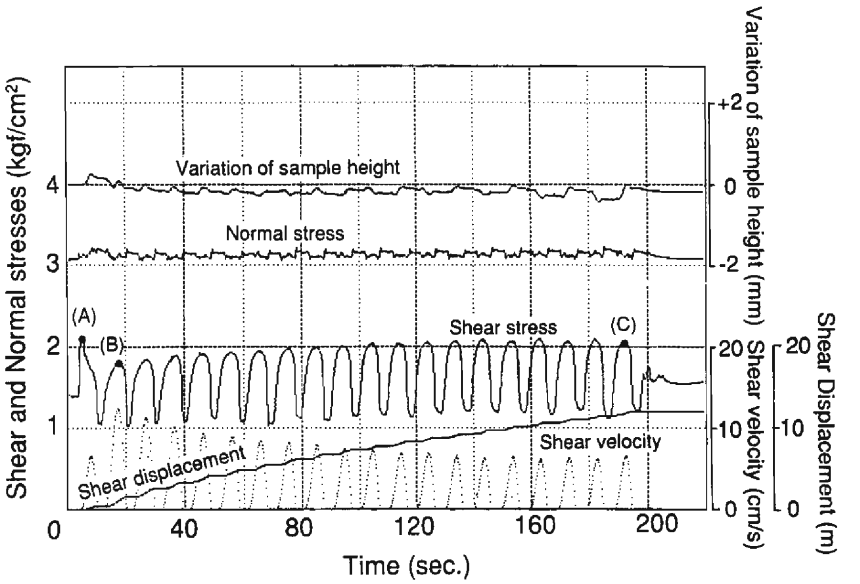

Fig. 14 Time series data of variation of sample height, normal stress, shear displacement, shear velocity in the cyclic shear stress loading test of the Galdian sample at the peak strength state (test No. 2–3).

height, normal stress, shear stress and shear velocity. The total shear displacement during the 20 cycles was about 12m. Time series data (test No. 2–3) of the variation of sample height, normal and shear stresses, shear velocity and shear displacement are shown in **Fig. 14.** Shearing velocity changed in proportion to the value of the cyclic loaded shear stress. In the first cycle, the peak of the shear velocity reached 8 cm/sec and then in the second and the third cycles it increased to 12 cm/sec. The peak velocity then gradually declined due to the increase of soil strength and reached 7 cm/sec in the 20th cycle.

After this stage, shearing with constant speed (0.02 cm/sec) was performed without changing the sample (test No. 2–4). **Fig. 15** is the result of this test. The residual friction angle was 28.6° after 400 cm displacement. After test No. 2–4, a cyclic shear loading test with constant normal stress was carried out (test No. 2–5). The stress path of this test is presented in **Fig. 16.** The measured dynamic friction angle was 31.4°. Logarithm of shear displacement versus the variation of sample height, normal stress, shear stress and shear velocity is presented in **Fig. 17.** Time series data of the variation of sample height, normal and shear stresses, shear displacement and shear velocity are shown in **Fig. 18.** Failure took place in the first cycle with low velocity and the total shear displacement during 20 cycles was about 80 cm. The maximum shear velocity was 2 cm/sec.

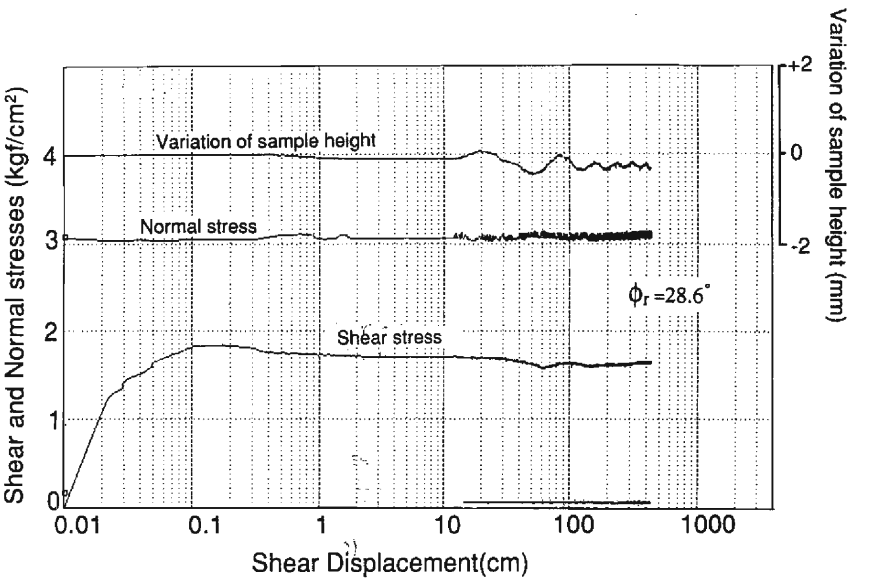

Fig. 15 Shear displacement (Log L) versus variation of sample height, normal stress, shear resistance and shear velocity in the constant speed shearing test of the Galdian sample after test No. 2-3 without changing the sample (test No. 2-4).

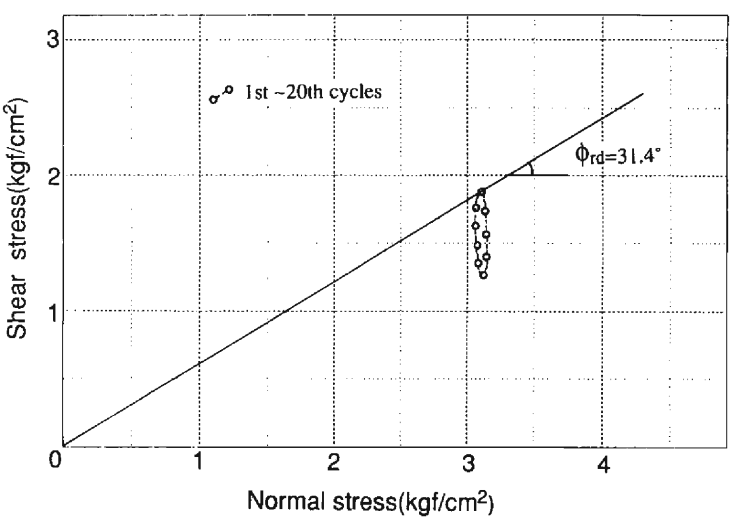

Fig. 16 Stress path of the cyclic shear stress loading test of the Galdian sample at the residual strength state (test No. 2-5).

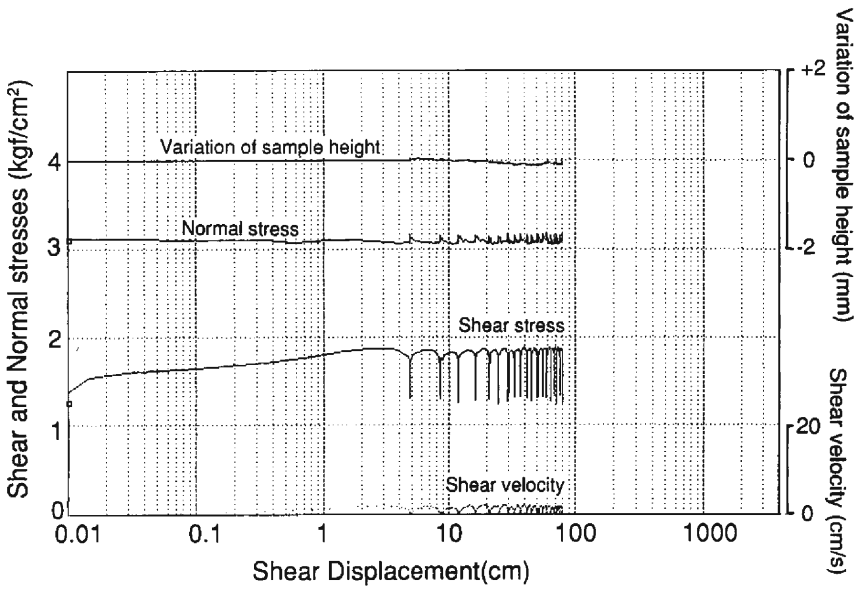

Fig. 17 Shear displacement (Log L) versus variation of sample height, normal stress, shear resistance and shear velocity in the cyclic shear stress loading test of the Galdian sample at the residual strength state (test No. 2–5).

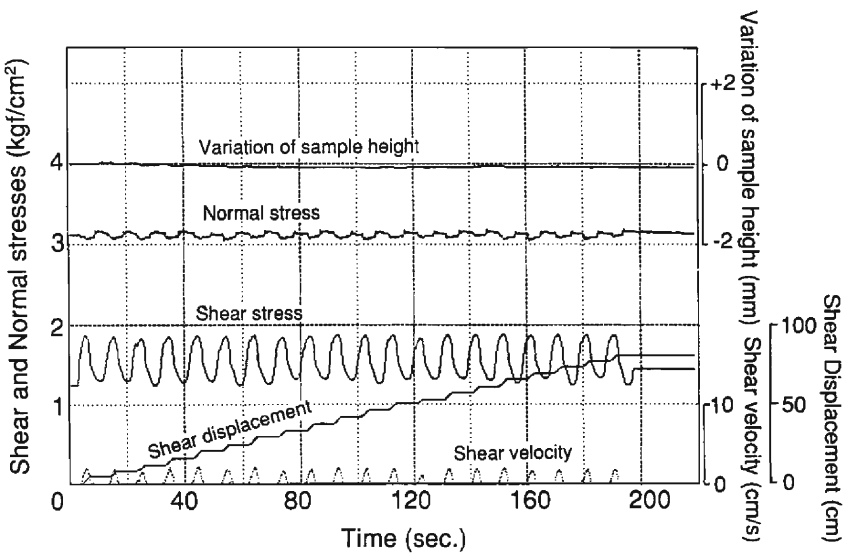

Fig. 18 Time series data of variation of sample height, normal stress, shear displacement, shear velocity in the cyclic shear stress loading test of the Galdian sample at the residual strength state (test No. 2–5).

6. Discussion

To apply the test results to the interpretation of the mechanism of the landslides, firstly, the parameters and their assumptions used in the discussion will be explained.

a) Dynamic friction angle: For discussing the shear strength of the soils obtained in these tests, the dynamic friction angle is the best index. However, it is not possible to obtain the dynamic friction angle from a single test. Therefore, we calculated it by assuming the sample as a cohesionless soil. This assumption may not be true, but the cohesion will not be so high because the samples were normally consolidated from the slurry state. The normal stress used in these tests was limited within 2.8～3.2 kgf/cm^2 and the discussion is also limited to this range of normal stress. Therefore, this assumption may be allowed.

The pore pressure was not considered in the calculation of the dynamic friction. Therefore this value is not the effective dynamic friction angle, it is the dynamic friction angle in the total stress concept.

b) Parameters of the landslides: For applying the tests results, the slope angle (θ) (approximated to be the same as the inclination of the sliding surface) on the studied landslides are considered as 20° in the upper slope (initial landslide meshed in **Fig. 3**) and 12° in the lower part (reactivating landslide, **Fig. 3**) of the Galdian landslide, and 20° for the Fatalak landslide (BB′ section in **Fig. 4**).

c) Pore pressure ratio: **Fig. 19** illustrates the initial stress and initial pore pressure before seismic loading. If the pore pressure is zero (hw=0) in the slope, its initial stress is expressed as point "A_0" on the line of the slope angle (θ) in the stress diagram b). When we give the initial stress (σ_0', τ_0) expressed as "A" in the ring shear test, it corresponds to the field situation of a certain pore pressure ratio. Therefore, we can calculate the pore pressure ratio and the ground water level in the examined slope corresponding to the initial stress given in the ring shear test as follows:

From **Fig. 19b**)

$$u=\sigma_0-\sigma_0'=\frac{\tau_0}{\tan\theta}-\frac{\tau_0}{\tan\alpha}, \tag{1}$$

where

u : pore pressure
σ_0 : initial total normal stress
σ_0' : initial effective normal stress
τ_0 : initial shear stress
θ : slope angle $=\tan^{-1}\frac{\tau_0}{\sigma_0}$
α : $\tan^{-1}\frac{\tau_0}{\sigma_0'}$

From **Fig. 19a**)

$$\tau_0=\gamma_t \cdot h \cdot \cos\theta \cdot \sin\theta, \tag{2}$$

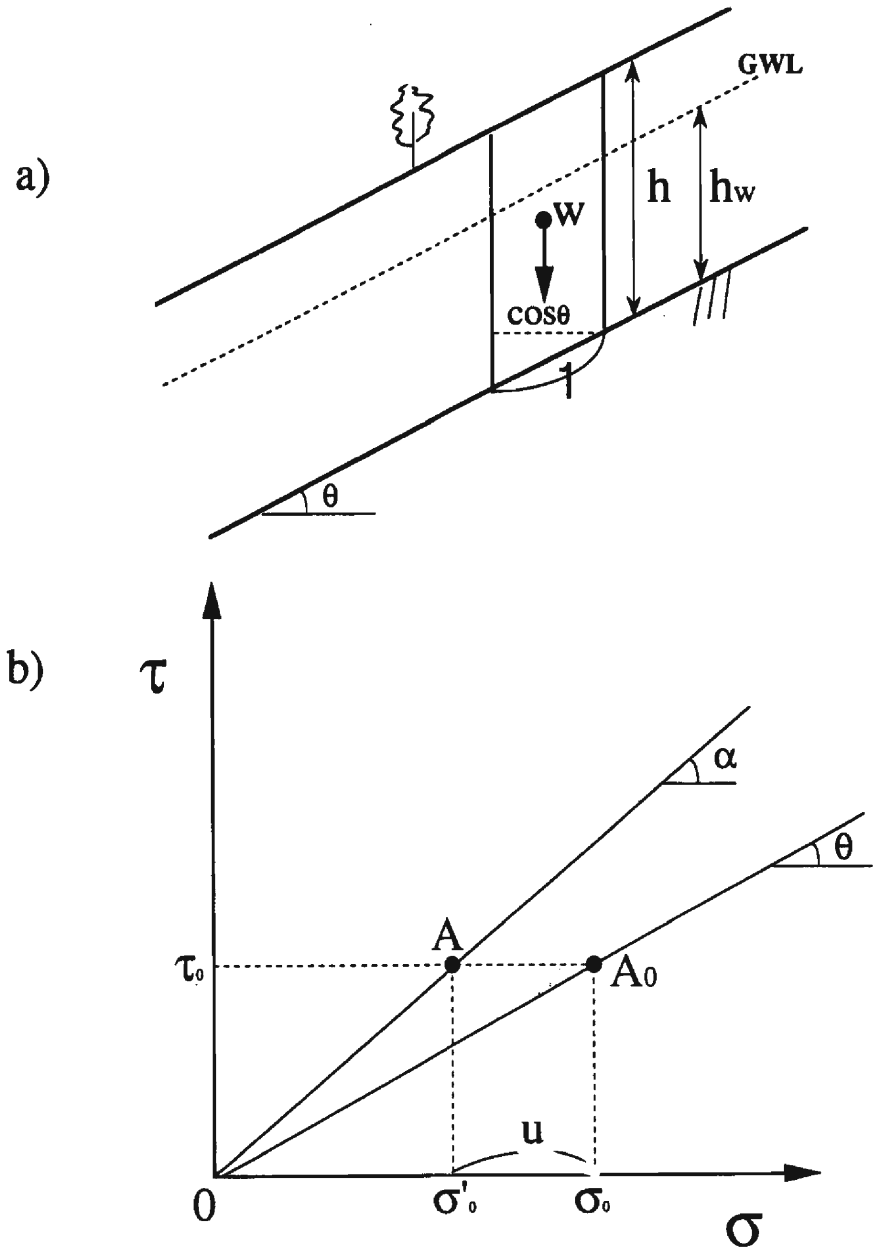

Fig. 19 Initial stress and initial pore pressure in the field and in the stress diagram.

where

γ_t : total unit weight

h : depth of the sliding surface.

Pore pressure ratio in the field is defined as

$$r_u=\frac{u}{\gamma_t \cdot h}. \tag{3}$$

Thus, the pore pressure ratio (r_{ut}) in the slope corresponding to the given initial stress in the test is obtained from Eqs. (1), (2) and (3) as

$$r_{ut}=\left(\frac{1}{\tan\theta}-\frac{1}{\tan\alpha}\right)\cos\theta \cdot \sin\theta=\cos^2\theta-\frac{\sigma_0'}{\tau_0}\cos\theta \cdot \sin\theta. \tag{4}$$

The ground water level (h_w) is obtained from r_{ut} as

$$h_w=\frac{\gamma_t \cdot h}{\gamma_w \cdot \cos^2\theta}\, r_{ut}, \tag{5}$$

where

$u=\gamma_w \cdot h_w \cdot \cos^2\theta$

γ_w : unit weight of water.

d) Seismic coefficient: The initial shear stress (τ_0) is expressed by Eq. (6) from **Fig. 6–a**) and the seismic stress necessary to cause failure (k_f) acting on a column of unit width in the slope (θ) is expressed by Eq. (7) from **Fig. 6–b**),

$$\tau_0=w \cdot \sin\theta, \tag{6}$$

$$k_f w=\sqrt{d\sigma_f^2+d\tau_f^2}. \tag{7}$$

From Eqs. (6) and (7),

$$k_f=\frac{\sqrt{d\sigma_f^2+d\tau_f^2}}{\tau_0}\sin\theta. \tag{8}$$

Using this equation, we can estimate the seismic coefficient (k_f) which is necessary to cause failure, from 1) slope angle (θ), 2) initial shear stress (τ_0) and the increment of shear stress ($d\tau_f$) at failure which are monitored by the shear load cell (I), 3) the monitored normal stress increment ($d\sigma_f$) obtained from the difference of two load cells (E and R). Using the pore pressure ratio and the seismic coefficient mentioned above, we can compare the test results to the observed phenomena in the landslides. A summary of the tests results is listed in **Table 2.**

Table 2 A summary of the test results.

Sample/Slope	$\alpha=\tan^{-1}(\tau_0/\sigma'_0)$	r_{ut}	ϕ_d	$d\tau_f$, $d\sigma_f$ (kgf/cm^2)	k_f
Fatalak sample (peak strength state)	24.7°	0.184	A) 1st cycle : 34.1°	0.70, 0.12	0.187
Slope angle=20° Depth of the sliding surface=20m			B) 2nd cycle : 25.9°	0.11, 0.07	0.034
			C) 20th cycle : 28.1°	0.25, 0.07	0.068
Galdian sample (peak strength state)	24.1°	0.166	A) 1st cycle : 33.5°	0.70, 0.06	0.174
Slope angle=20° Depth of the sliding surface=20–25m			B) 2nd cycle : 30.2°	0.45, 0.06	0.113
			C) 20th cycle : 33.0°	0.66, 0.06	0.165

τ_0, σ'_0: Initial shear stress effective normal stress before test, r_{ut}: Pore pressure ratio in the slope corresponding to the given initial stress in the tests, k_f: Seismic coefficient necessary to cause failure, $d\tau_f$ and $d\sigma_f$: Stress increment at failure, ϕ_d: Dynamic friction angle, A, B and C: Stress points which are indicated in the time series graphs of the tests (Figs. 11 and 14).

6.1 Fatalak Landslide

In **Fig. 9** (test No. 1–3) the dynamic friction angle in the first cycle (peak strength state) reached 34.1° and dropped to 25.9° in the second cycle, and then went up to 28.1° in the 20th cycle. This increase could be due to grain crushing during shearing as suggested by H. Fukuoka[7]. Using the slope angle of 20° and Eq. (4), we can calculate the pore pressure ratio (r_{ut}) corresponding to the initial stress condition of test No. 1–3. It was 0.184 as indicated in **Table 2**, which corresponds to the ground water level of 8.2m above the sliding surface for the average depth of 20m from Eq. (5). Real pore pressure ratio in the field was not known, but about 1/2–1/3 saturation of the landslide mass is probably the case. By substituting the stress increment at failure and the slope angle into Eq. (8), we can obtain the seismic coefficient (k_f) necessary to cause failure. In the first cyclic cycle, (point (A) in **Fig. 11**) the seismic coefficient necessary to cause failure (k_f) became 0.187. This implies that, the peak strength should be greater than 2.0 kgf/cm^2 in order to resist the earthquake loading with the seismic coefficient of 0.187. The seismic coefficient (k_f) necessary to cause failure in the second cycle was 0.034 (point (B) in **Fig. 11**). The shear resistance showed an increase (**Figs. 10, 11**) toward the 20th cycle, but never reached the peak state value. The seismic coefficient (k_f) necessary to cause failure in the 20th cycle was 0.068 ($\tau_{max}=1.55$ kgf/cm^2). During the main shock, the ground acceleration of the earthquake at the Abbar strong motion station was estimated as 0.65g[1]. By applying the attenuation equation for the Manjil earthquake suggested by Niazi *et al.*[1], the peak ground acceleration that reached the Fatalak landslide was calculated as 416 gal (k=0.425) which was far greater than the seismic coefficient necessary to cause failure obtained from the test ($k_f=0.187$). The loss of strength between the first cycle and the second cycle must be one of the main causes of high speed failure as observed during the earthquake. The moved soils traveled downward and buried the stream at the foot of the slope and stopped at the bottom of the opposite flank, and thus recovered the stability of this

landslide during further shaking.

6.2 Galdian Landslide

Initial landslide in the upper steep slope: In **Fig. 12** (test No. 2–3) the dynamic friction angle in the first cycle reached 33.5° and in the second cycle dropped to 30.2°, and then gradually recovered to 33.0° in the 20th cycle. This recovery of the dynamic friction angle could be due to grain crashing during shearing, as in the Fatalak sample. In the first cycle, (point (A) in **Fig. 14**) the seismic coefficient (k_f) necessary to cause failure was 0.174. This value was measured under the condition of pore pressure ratio (r_{ut}) of 0.166 that corresponds to the ground water levels of 7.7m and 9.6m for the depth of the sliding surfaces of 20m and 25m respectively. In the second cycle a decrease in the soil strength was observed, and the seismic coefficient (k_f) necessary to cause failure in the second cycle (point (B) in **Fig. 14**) was 0.113, but shear strength gradually increased in the following cycles of test (**Figs. 13, 14**) and reached the maximum of $\tau_{max}=2.04$ kgf/cm^2 in the 20th cycle which corresponds to the k_f of 0.165. The peak ground acceleration that reached the Galdian landslide was estimated as 539 gal, ($k=0.550$)[1]. It was far greater than the critical value ($k_f=0.174$) obtained from the test. The loss of shear strength between the first cycle and the second cycle must be one of the main causes of the high velocity failure that took place at the upper part with steeper slope (meshed part in **Fig. 3**) of the Galdian landslide during the main shock of the earthquake.

Reactivating landslide on the lower gentle slope: As indicated in **Fig. 2** the old landslide almost covered the whole of the lower part of the Galdian landslide with an average slope angle of 12°. The sliding surface of the old landslide was considered to be at the residual strength state. Two possibilities can be considered to explain the main cause of the continuing intermittent motion of the lower part of the Galdian landslide during the following two weeks after the main shock.

1) As suggested by Ishihara[8], the slid masses of the upper and steeper part (meshed part in **Fig. 3**) created the additional force to load the downslope soil masses. The damage to the outlets of the springs in the upper part enabled the penetration of spring water downward. The ground water level of the lower part of the landslide might have been near the ground surface (after the failure in the upper part, two small ponds became visible at the slope surface). Therefore, let us assume that the pore pressure ratio (r_u) at the sliding surface reached the value of 0.455 (**Table 3**) corresponding to this situation. In this condition the seismic coefficient (k_f) necessary to cause failure was calculated to be 0.128 using the dynamic friction angle of 31.4° obtained from the test result (**Fig. 16**).

2) The sample employed was taken from the bottom of scarp, but not from the sliding surface of the reactivated old landslide. In the old landslide a more clayey sliding surface having a smaller friction angle was probably formed by long-term weathering. Assuming that the real value of the residual friction angle of the sliding surface of the old landslide was 20° or 24°, in the case of pore pressure ratio in the field (r_u) of 0.166 (the same value as used in the examination of the initial landslide in **Table 2**), the seismic coefficients (k_f) necessary to cause failure was calculated to be 0.098 for the residual friction angle of 20°, and to be 0.165 for the residual friction angle of 24° (**Table 3**). For both of these possibilities the aftershocks

Table 3 Combination of pore pressure ratio and the dynamic friction angle to give the value of k_f smaller than those during the aftershocks.

Sample/Slope	r_u (Assumed)	ϕ_{rd}	$d\tau_f$, $d\sigma_f$ (kgf/cm^2)	k_f
Galdian sample (residual strength state)	0.455	1st–20th cycles : 31.4°	0.51, 0	0.128
Slope angle = 12°	0.166	20° (Assumed)	0.39, 0	0.098
Depth of the sliding surface = 20m	0.166	24° (Assumed)	0.66, 0	0.165

r_u: Pore pressure ratio assumed in the discussion, k_f: Seismic coefficient necessary to cause failure, $d\tau_f$ and $d\sigma_f$: Stress increment at failure, ϕ_{rd}: Residual dynamic friction angle.

within two weeks with ground acceleration of 77–180 gal (k=0.079–0.183) were large enough to cause the intermittent motion that was observed during two weeks after the main shock in the lower part of the Galdian landslide.

7. Conclusion

Two sites of the major ladslides triggered by the 1990 Iran earthquake were investigated from the points of view of field survey and soil dynamics. Newly-developed cyclic ring shear apparatus was used to reproduce the stress condition during the earthquake. The results of tests for the samples from the Fatalak landslide and the Galdian landslide at the peak strength state confirmed that ground acceleration of 0.425–0.550g during the earthquake that hit the Galdian and the Fatalak regions were large enough to cause failure with high velocity in the Fatalak landslide and in the upper and steeper slope of the Galdian landslide. In the case of the Fatalak landslide, the moved soil masses reached the opposite flank and became stable. Test results of the sample at the residual strength state (dynamic residual friction angle of 31.4°) of the Galdian landslide confirmed that if the pore pressure ratio had reached 0.455 (due to the new condition of the ground water regime after the main shock) or if the sliding surface in the old landslide had a smaller friction angle of 20° to 24° (in the case of a pore pressure ratio of 0.166 : the same value as used for the initial upper landslide) the ground acceleration of aftershocks of 77–180 gal within the following two weeks should have been large enough to cause intermittent motion in the lower part of the Galdian landslide.

Acknowledgment

The authors are grateful to Dr. M. A. Nogol Sadat of the Geological Survey of Iran for field survey data, and Mr. M. Taghian, Mr. M. Mozaffari and A. Khani of the Ministry of Jahad, Iran-Shahrood for their helpful assistance in sampling and field survey. The authors thank Dr. H. Fukuoka of the Disaster Prevention Research Institute, Kyoto University for his

contribution to computer programming for the cyclic loading ring shear tests.

References

1) Niazi, M., Y. Bozorgnia : The 1990 Manjil, Iran Earthquake : Geology and Seismology Overview, PGA Attenuation, and Observed Damage, Bulletin of the Seismological Society of America, Vol. 82, No. 2, 1992, pp. 774–799.
2) M. A. Nogol Sadat : Geological Survey of Iran, Personal comm., July 20, 1991.
3) Hungr, O., N. R. Morgenstern : High Velocity Ring Shear Tests on Sand, Géotechnique, Vol. 34, 1984, pp. 415–421.
4) Sassa, K., M. Shima, H. Hiura, A. Nakagawa and A. Suemine : Development of Ring Shear Type Debris Flow Apparatus, Report of Grant-in-Aid for Scientific Research By Japanese Min. of Education, Science and Culture (No. 57860028), 1984, 30 pages.
5) Sassa, K., H. Fukuoka, C. Vibert, M. Shima : Development of a High-Speed High-Stress Ring Shear Apparatus and Shear Strength Reduction at Rapid Loading in Landslides, Annuals, Disas. Prev. Res. Ins., Kyoto Univ. 32, No. B-1, 1989, pp. 165-185 (in Japanese).
6) Sassa, K. : Access to the Dynamics of Landslides During Earthquakes by a New Cyclic Loading High-Speed Ring Shear Apparatus, Theme Address, Sixth International Symposium on Landslides, Christchurch, New Zealand, "Landslides", Vol. 3, Bulkema Ltd., 1992, 20 pages. (in print).
7) Fukuoka, H. : Variation of the Friction Angle of Granular Material in the High-Speed High-Stress Ring Shear Apparatus, —Influence of re-orientation, alignment and crushing of grains during shear—, Bull. Disas. Prev. Res. Ins., Kyoto Univ., Vol. 41, Part 4, No. 362, 1991, pp. 243–279.
8) Ishihara, K. : Manjil Earthquake of 21 June 1990, Iran, International Newsletter, "Landslide News", Japan Landslide Society, No. 5, 1991, pp. 2–4.
9) Ishihara, K. : Stability of Natural Deposits During Earthquake, Proc. 11th International Conference on Soil Mechanics and Foundation Engineering, San Francisco, Vol. 1, 1985, pp. 321–375.